OPEN ACCESS

Global Journal of Research in Engineering & Computer Sciences
ISSN: 2583-2727 (Online)
Volume 02| Issue 02 | March-April | 2022
Journal homepage: https://gjrpublication.com/journals/

Original Research Article

A Complete study and review of Characterization Techniques of Nano materials

*Dr. E.N.Ganesh

Dean School of Engineering VISTAS Chennai

Submission Date: 17th March 2022 | **Published Date:** 30th March 2022

***Corresponding author:** Dr. E.N.Ganesh

Abstract

Nano-materials are currently gaining a lot of prominence due to their unique properties and applications in various fields. Much information is available in the literature on the synthesis and applications of these materials such as carbon nano tubes, nano capsules for drug delivery, bio-synthesized gold and silver nano particles etc. However, in each case, characterization carries a lot of importance, particularly, validation by transmission electron microscopic techniques. In this paper, an attempt has been made to elucidate x-ray diffraction and different electron microscopic techniques such as FEG SEM, Environmental SEM, TEM along with EDS, AFM and FIB etc. which are used for the characterization of nano-materials. Also included are sample preparation techniques for the observation of these materials using electron microscopy.

Keywords: Scanning Electron Microscope; Atom force Microscope; Nanomaterial; Electron Microscope; XRay Diffraction;

INTRODUCTION

Nano materials are emerging family of novel materials that could be designed for specific properties. The various properties – mechanical, thermal, chemical and electrical - could be tailored for specific applications. For example, nano-particle re-enforced polymers may be used to replace metallic components in automobile industry for reduced fuel consumption and CO_2 emission, increasing the efficiency by 10%. Also, they can be used to make environmental friendly wear resistant tyres. Nano porous materials/filters can be used for faster chemical synthesis. Lighter, stronger and thermally stable nano-materials are very useful for fuel efficient lifting of space vehicle payloads into orbit and reduced dependence on solar power.

These materials are also useful in nanolithography for improved printing ability. Nano coatings are useful for cutting tools and thermal insulation. Nano YSZ coating is used for radiation absorption. Structural carbon and ceramic nano materials are significantly stronger than steel and have better heat resistance. Again, to have better high temperature stability and strength, Ni base super alloys are made by dispersing 1 -100 nm oxide particles for aero-space applications [1]. In the field of medicine, possibilities are immense.

Carbon nano tubes are special nano-materials discovered by Iijima in 1991[1]. They have better electrical conductivity than copper, exceptional mechanical strength and high flexibility. These materials are used in chemical sensors, electronic IC circuits, hydrogen storage devices and temperature sensors. The strength of nano tubular materials can be increased by assembling them in the form of ropes of 20-30 nm diameter and several micrometers in length. Metal nano-wires and nano-particles are commonly formed by employing a template.

One has to observe and characterize these nano materials in order to design a new material with specific properties and applications as per the requirements. Different techniques are available for the characterization of nano materials [2]. They are: X-Ray Diffraction (XRD), Electron Diffraction, Electron Microscopic techniques like Field Emission Gun Scanning Electron Microscopy (FEG SEM), Environmental SEM, Transmission Electron Microscopy (TEM) along with Energy Dispersive System (EDS), Atomic Force Microscopy (AFM), and Focused Ion Beam (FIB). These methods aim at determining the crystal structure, defect structure, chemical analysis, phase identification, crystal or grain size etc. All

these techniques are widely used for the characterization of nano-materials and will be explained briefly in the following sections.

X-Ray Diffraction

X-ray analysis has established the crystal structures of several elements and compounds. Electromagnetic waves of wavelength comparable to crystal lattice spacing are strongly diffracted by a crystal. Analysis of the diffraction pattern allows us to obtain information such as crystal structure, lattice parameter, crystal orientation and particle size. Diffraction is governed by the Bragg formula:

$$2d \sin \vartheta = n \lambda \qquad (1)$$

Here d is the inter-planar spacing, θ is the angle of diffraction, λ is the wavelength of the incident beam and n is the order of diffraction.

In a typical set up, a collimated beam of x-rays is incident on the sample. The intensity of the diffracted x-rays is measured as a function of the diffracted angle 2θ. (See Fig.1)

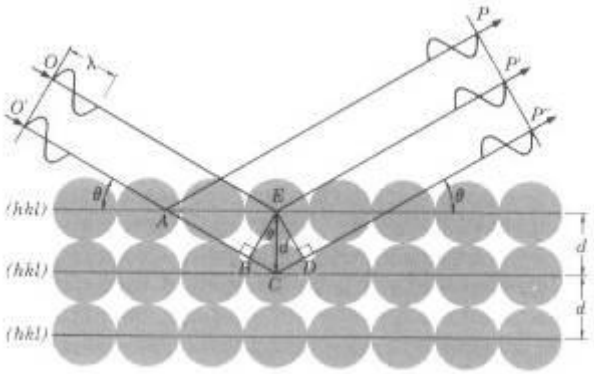

Fig.1: Diffraction of x-rays by crystal planes

The intensities of the diffracted beams provide information about the atomic arrangement. The sharpness and shape of the reflections are related to the perfection of the crystal. The two basic procedures involve the use of either a single crystal sample with monochromatic or white radiation, or a powder sample in conjunction with monochromatic radiation. With single crystal, a lot of information about the structure can be obtained. On the other hand, single crystals are difficult to get and determination of orientation of crystal is cumbersome.

A typical x-Ray powder diffraction pattern (Intensity Vs 2θ) is given in Fig.2.

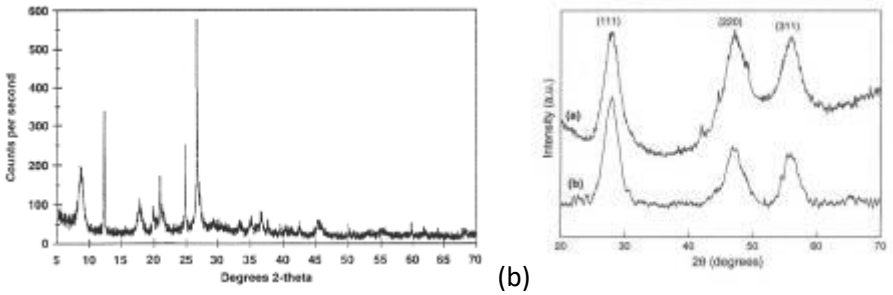

Fig.2: (a)X-ray powder diffraction plot. Peak positions occur where the x-ray beam has been diffracted by the crystal lattice; (b) Line broadening due to nano size [3]

Knowing the x-ray wavelength used and measuring θ, d can be evaluated.

For cubic crystals, we have, $d = \dfrac{a}{\sqrt{h^2 + k^2 + l^2}}$ where a is the lattice parameter and h,k,l are the miller indices of the diffracting planes. The ratios of $\sin^2\theta$ are: for BCC - 2:4:6…; FCC- 3:4:8:11:…; DC: 3:8:11:16:…. From this analysis, it is possible to identify the Bravais lattice and determine the lattice parameter. For non-cubic structures, more complex methods and methods based on reciprocal lattice are available. Single crystal diffraction patterns are also

capable of providing data on the crystal structure. Besides, they also reveal the state of perfection of the crystal. One can assess the proportion of phases in a multi-phase solid. X-ray diffraction techniques are suitable for studying amorphous solids.

As mentioned earlier, x-ray diffraction techniques can yield information on particle size (actually, size of coherently diffracting domains). Smaller the particle size, broader is the diffraction peak. Nano particles cause appreciable broadening of diffraction lines. The breadth *B* of a diffraction line (measured as the width at half maximum intensity or as integral breadth) is related to the particle size *t* via the Scherrer formula:

$$t = \frac{0.9\lambda}{BCos\theta} \qquad (2)$$

It should be noted that *B* however has contributions from instrument, lattice strain and stacking faults which are to be accounted for to get the breadth due to small particle size. In a similar fashion, lattice strains, the density of stacking faults, dislocation density etc can be computed.

Energy dispersive X-ray spectroscopy (EDS) is an analytical technique used for the elemental analysis or chemical characterization of a sample. It relies on the investigation of a sample through interactions between electromagnetic radiation or particles and matter. X-rays emitted by the matter as a result of the interaction are analysed. The underlying fundamental principle is that each element has a unique atomic structure allowing emission of x-rays that are characteristic of the element's atomic structure to be identified uniquely from each other. To stimulate the emission of characteristic x-rays from a specimen, a high energy beam of charged particles such as electrons or protons, or a beam of x-rays, is focused into the sample being studied.

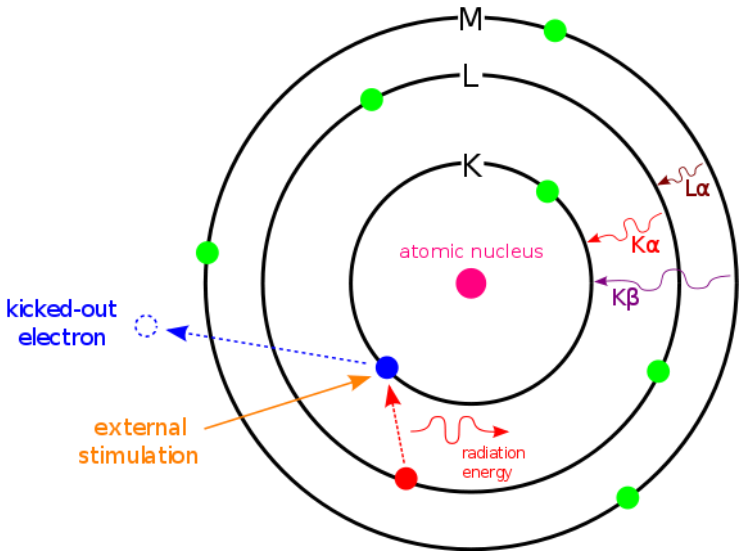

Fig.3: Origin of different radiations

At rest, an atom within the sample contains ground state (or unexcited) electrons in discrete energy levels or electron shells bound to the nucleus. The incident beam may excite an electron in an inner shell, ejecting it from the shell. An electron from an outer, higher-energy shell then fills the hole, and the difference in energy between the higher-energy shell and the lower energy shell may be released in the form of an x-ray characteristic radiation (Fig.3). The number and energy of the x-rays emitted from the specimen can be measured by an energy dispersive spectrometer. As the energy of the x-rays is characteristic of the difference in energy between the two shells, and of the atomic structure of the element from which they were emitted, this allows the elemental composition of the specimen to be measured as shown in Fig. 4.

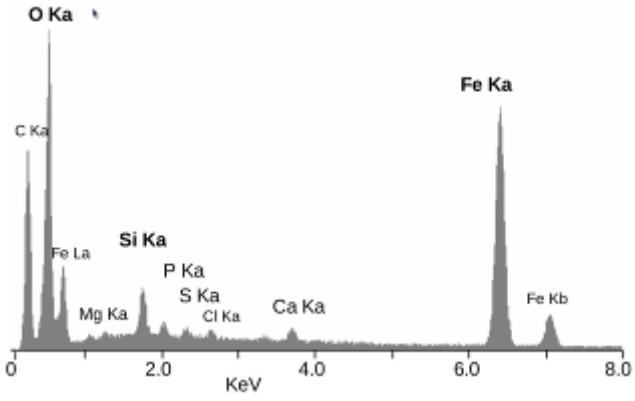

Fig.4: A typical EDS profile of an Iron oxide sample [4]

EDS systems can be attached to both TEM and SEM for carrying out elemental analysis. A number of free-standing EDS systems also exist. However, EDS systems are most commonly found on scanning electron microscopes (SEM-EDS) and electron microprobes.

The excess energy of the electron that migrates to an inner shell to fill the newly-created hole can do more than emit an x-rays. Often, instead of x-ray emission, the excess energy is transferred to a third electron from a further outer shell, prompting its ejection as shown in Fig.3. This ejected species is called an Auger electron, and the method for its analysis is known as Auger Electron Spectroscopy (AES). X-ray Photoelectron Spectroscopy (XPS) is also similat to EDS. It utilizes the ejected electrons in a manner similar to that of AES. Information on the quantity and kinetic energy of ejected electrons is used to determine the binding energy of these now-liberated electrons, which is element-specific and allows chemical characterization of a sample.

EDS is often contrasted with its spectroscopic counterpart, WDS (Wavelength-Dispersive x-ray Spectroscopy). WDS differs from EDS in that it uses the diffraction patterns created by radiation-matter interaction as its raw data. WDS has a much finer spectral resolution than EDS. In WDS only one element can be analyzed at a time, while EDS gathers a spectrum of all elements, within limits, of a sample.

XRD, with or without EDS/WDS is a simple and useful technique to derive a lot of information, particularly with regards to estimation of the size of nano-particles. A disadvantage of XRD is the low intensity of diffracted beams for low atomic number materials.

Electron Diffraction

Electron and neutron diffraction methods operate on the same principle as x-ray diffraction but the three techniques differ from each other in some aspects, particularly in the mechanism of scattering leading to the formation of diffracted beams. This behaviour makes them uniquely applicable in different applications. For example, neutron diffraction is suitable for studying magnetic properties of solids which cannot be investigated by electron and x-ray diffraction techniques. However, neutron sources are uncommon and expensive and discussion here is limited to electron diffraction. The wavelength of a beam of electrons is a function of the accelerating voltage in an electron gun and is given by:

$$\lambda = \sqrt{\frac{150}{V}} \qquad (3)$$

where, λ is in Å and V is in volts. For V = 10,000 volts, λ = 0.12 Å and for V = 40,000volts, λ = 0.06 Å. Thus the electron diffraction wavelengths are much smaller compared to x-ray diffraction wavelengths which are in the range 0.7 – 2.2 Å. An electron diffraction pattern is therefore confined to very small θ values.

The atomic scattering factors (f) for electrons and x-rays are related by the equation:

$$f_{ele} = (Z - f_{x-rays})\frac{\lambda^2}{\sin^2\theta} \qquad (4)$$

Where Z is the atomic number. It can be seen that $f_{ele} \approx 10^3 f_{x\text{-}ray}$ and the corresponding line/spot intensities in diffraction patterns of x-rays and electrons are in the proportion of $\approx 1{:}10^6$. Therefore, in order to obtain the same measurable intensity of diffraction, the size of the specimen must be varied according to the radiation used. If the linear dimension of the specimen for x-ray examination is 1mm, it can be about 10^{-5} mm for electron diffraction. Electron

diffraction is therefore ideally suited for study of thin films, oxidation products, etc, which is not possible or difficult by x-ray diffraction techniques.

The electron diffraction pattern consists of spots or rings similar to x-ray diffraction pattern and can be indexed in a similar way by using the equation: $L\lambda = rd$; where $L\lambda$ is a camera constant, r is the distance between centre of the diffraction pattern and the diffraction spot or ring radius. The geometry is identical for x-ray and electron diffraction which is depicted in Fig. 5 from which the Bragg law can be easily derived.

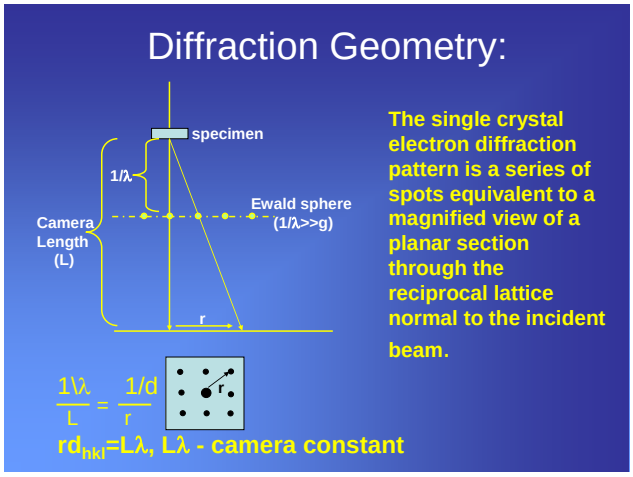

Fig.5: Geometry of X-ray and Electron Diffraction

Scanning Electron Microscopy

The scanning electron microscope (SEM) is a type of electron microscope that images the sample surface by scanning it with a high-energy beam of electrons in a raster scan pattern. The electrons interact with the atoms that make up the sample producing signals that contain information about the sample's surface topography, composition and other properties such as electrical conductivity as shown in Fig. 6.

The electron beam hits the sample, producing secondary electrons from the sample. These electrons are collected by a secondary detector or a backscatter detector, converted to a voltage, and amplified. The amplified voltage is applied to the grid of the CRT and causes the intensity of the spot of light to change. The image consists of thousands of spots of varying intensity on the screen of a CRT that correspond to the topography of the sample. The types of signals produced by an SEM include secondary electrons, back-scattered electrons (BSE), characteristic x-rays, light (cathodoluminescence), specimen current and transmitted electrons. Secondary electron detectors are common in all SEMs, but it is rare that a single machine would have detectors for all possible signals. The signals result from interactions of the electron beam with atoms at or near the surface of the sample. In the most common or standard detection mode, secondary electron imaging or SEI, the SEM can produce very high-resolution images of a sample surface, revealing details about less than 1 to 5 nm in size.

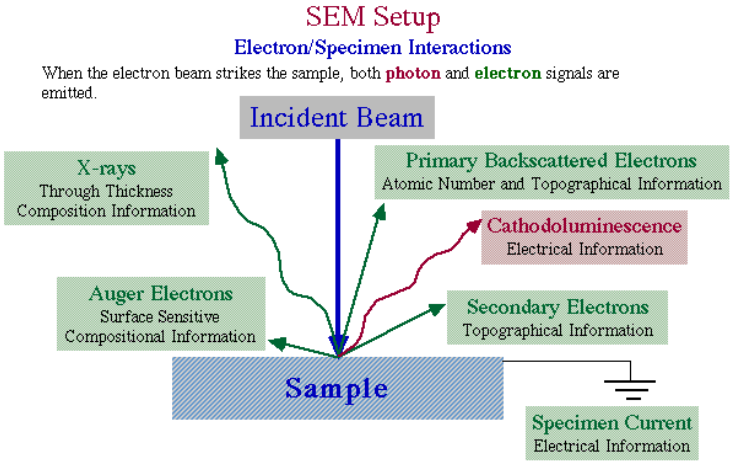

Fig.6 (a): SEM set up (above) (b) Equipment (below)

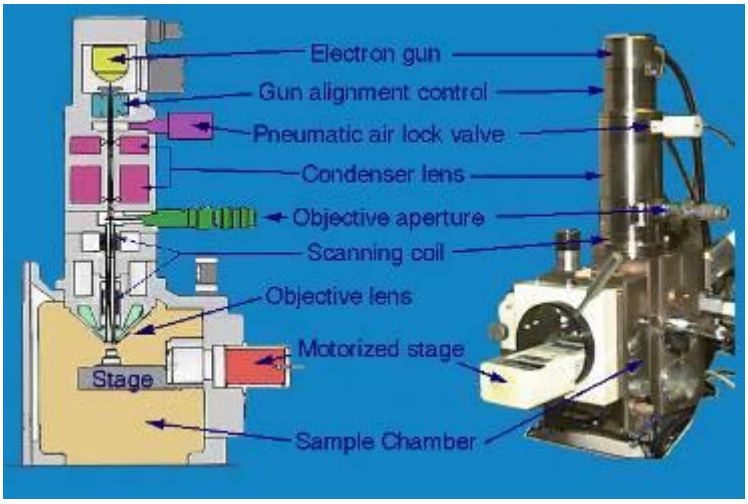

Due to the very narrow electron beam, SEM micrographs have a large depth of field yielding a characteristic three-dimensional appearance useful for understanding the surface structure of a sample. This is exemplified by the micrograph of pollen shown in the Fig.7. A wide range of magnifications is possible, from about 10 times to more than 500,000 times, about 250 times the magnification limit of the best light microscopes.

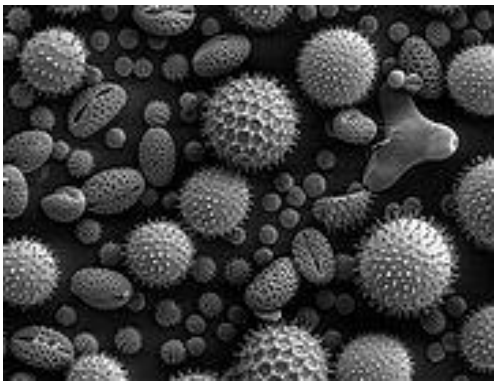

Fig.7: SEM picture of pollen grains show the characteristic depth of field of SEM micrographs

Back-scattered electrons (BSE) are beam electrons that are reflected from the sample by elastic scattering. BSE are often used in analytical SEM along with the spectra made from the characteristic x-rays. Because the intensity of the BSE signal is strongly related to the atomic number (*Z*) of the specimen, BSE images can provide information about the distribution of different elements in the sample. For the same reason, BSE imaging can image, for example, colloidal gold immuno-labels of 5 or 10 nm diameter which would otherwise be difficult or impossible to detect in secondary electron images in biological specimens. Characteristic x-rays are emitted when the electron beam removes an inner shell electron from the sample, causing a higher energy electron to fill the shell and release energy. These characteristic x-rays are used to identify the composition and measure the abundance of elements in the sample, as already described under EDS in Section 1. X-ray Diffraction.

Sample preparation for SEM: All samples must also be of an appropriate size to fit in the specimen chamber and are generally mounted rigidly on a specimen holder called a specimen stub. Several models of SEM can examine any part of 15 cm sample, and some can tilt an object of that size to 45°. For conventional imaging in the SEM, specimens must be *electrically conductive*, at least at the surface, and *electrically grounded* to prevent the accumulation of *electrostatic charge* at the surface. Metal objects require little special preparation for SEM except for cleaning and mounting on a specimen stub. Nonconductive specimens tend to charge when scanned by the electron beam, and especially in secondary electron imaging mode, this causes scanning faults and other image artifacts. They are therefore usually coated with an ultrathin coating of electrically-conducting material, commonly gold, deposited on the sample either by low vacuum *sputter coating* or by high vacuum evaporation. Conductive materials in current use for specimen coating include *gold*, gold/*palladium* alloy, *platinum*, *osmium*, *iridium*, *tungsten*, *chromium* and *graphite* [5]. Coating prevents the accumulation of *static electric charge* on the specimen during electron irradiation. An alternative to coating for some biological samples is to increase the bulk conductivity of the material by impregnation with osmium using variants of the OTO *staining* method (O-osmium, T-thiocarbohydrazide, O-osmium) [6,7]. Non conducting specimens may be imaged uncoated using specialized SEM instrumentation such as the "Environmental SEM" (ESEM) or field emission gun (FEG) SEMs

operated at low voltage. Environmental SEM instruments place the specimen in a relatively high pressure chamber where the working distance is short and the electron optical column is differentially pumped to keep the vacuum adequately low at the electron gun. The high pressure region around the sample in the ESEM neutralizes charge and provides an amplification of the secondary electron signal. Low voltage SEM of non-conducting specimens can be operationally difficult to accomplish in a conventional SEM and is typically a research application for specimens that are sensitive to the process of applying conductive coatings. Low-voltage SEM is typically conducted in an FEG-SEM because the FEG is capable of producing high primary electron brightness even at low accelerating potentials. Operating conditions must be adjusted such that the local space charge is at or near neutral with adequate low voltage secondary electrons being available to neutralize any positively charged surface sites. Embedding the sample in a *resin* with further polishing to a mirror-like finish can be used for both biological and materials specimens when imaging in backscattered electrons or when doing quantitative X-ray microanalysis. Fig.8 is an example of a typical SEM picture of a biological sample with conductive gold coating.

Fig.8: An insect coated in gold, having been prepared for viewing with a scanning electron microscope

Fractography is the study of fractured surfaces that can be done in a light microscope or more commonly on an SEM. SEM is being widely employed to investigate fracture modes and fracture mechanisms. The fractured surface is cut to a suitable size, cleaned of any organic residues, and mounted on a specimen holder for viewing in the SEM. Representative fractgraphs are shown in Fig.9.

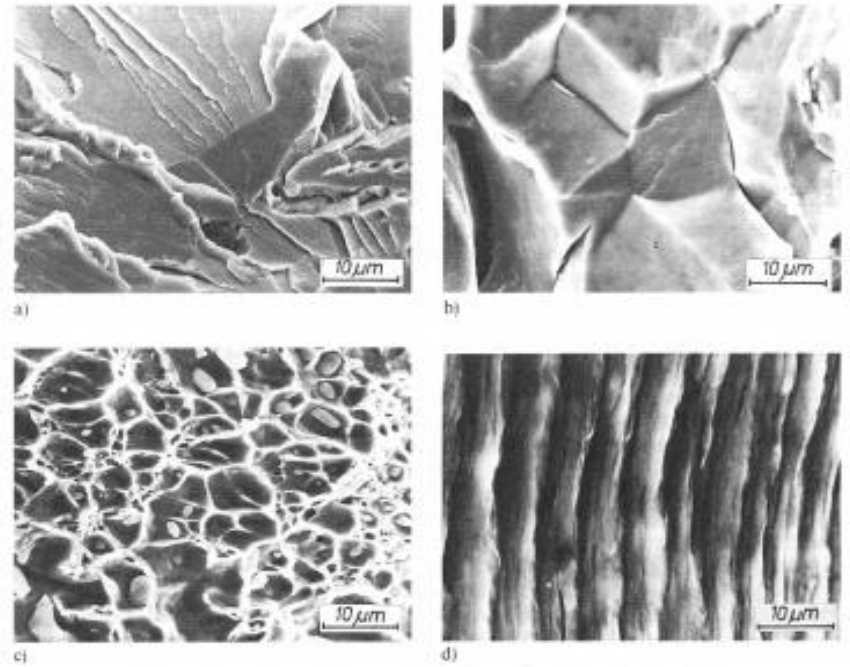

Fig. 9: a) Transgranular cleavage fracture, b) intercrystalline cleavage fracture c) dimple fracture (transgranular), d) fatigue fracture

Detection of backscattered electrons: Backscattered electrons (BSE) consist of high-energy electrons originating in the electron beam that are reflected or back-scattered out of the specimen interaction volume by elastic scattering interactions with specimen atoms. Since heavy elements (high atomic number) backscatter electrons more strongly than light elements (low atomic number), and thus appear brighter in the image, BSE are used to detect contrast between areas with different chemical compositions [8]. Dedicated backscattered electron detectors are positioned above the sample in a "doughnut" type arrangement, concentric with the electron beam, maximising the solid angle of collection. BSE detectors are usually either of scintillator or semiconductor types. When all parts of the detector are used to collect electrons symmetrically about the beam, atomic number contrast is produced. However, strong topographic contrast is produced by collecting back-scattered electrons from one side above the specimen using an asymmetrical, directional BSE detector; the resulting contrast appears as illumination of the topography from that side. Semiconductor detectors can be made in radial segments that can be switched in or out to control the type of contrast produced and its directionality. An example is given in the Fig.10.

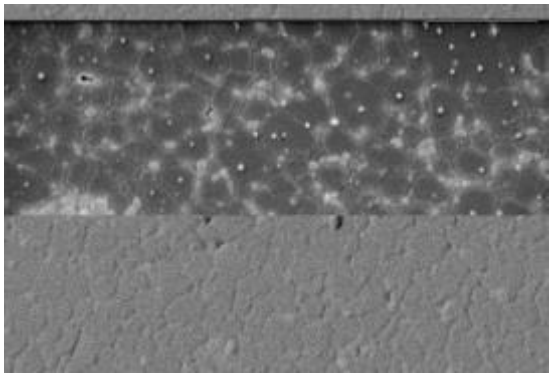

Fig. 10: Comparison of SEM techniques: Top: backscattered electron analysis – composition; Bottom: secondary electron analysis – topography

Backscattered electrons can also be used to form an Electron Back Scatter Diffraction (EBSD) image that can be used to determine the crystallographic structure of the specimen. Fig.11 shows a typical EBSD picture of a polished sample.

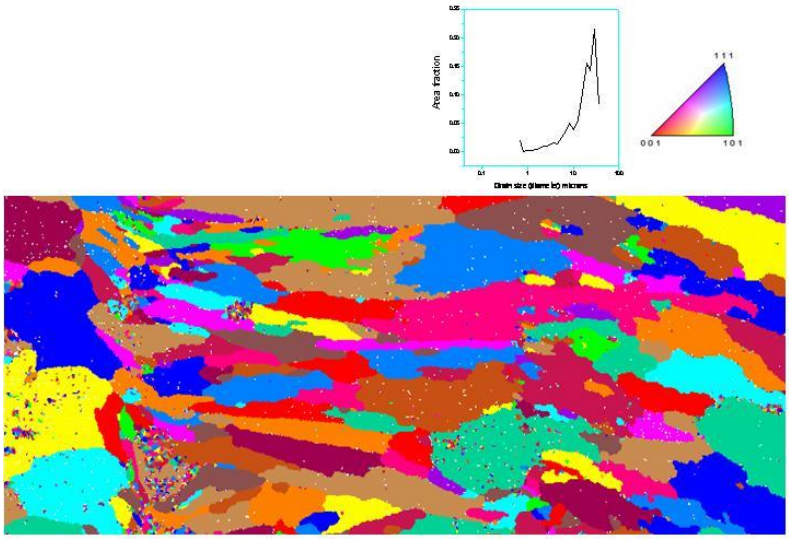

Fig.11: Example of Orientation Image Microscopy (OIM) using EBSD detector
(Grain orientations in Fe-Sn clad system)

Transmission Electron Microscopy

The basic operation in a Transmission Electron Microscope (TEM) is that electrons generated from an electron gun are scattered by the sample. The scattered electrons are focused using electron optic lenses to finally form images. The imaging modes can be controlled by the use of an aperture. If most of the scattered electrons are allowed through, we get *Bright Field* image. If specific scattered beams are selected, the image is known as a *Dark Field* image. In addition, a TEM can also be used for chemical analysis. Electrons scattered from the sample are collected on a CRT to form the image. The resolution is a few nm and magnification ~ 10X to 5,00,000X. Selected Area Diffraction (SAD) or Convergent Beam Electron Diffraction (CBED) is used to characterize the crystalline nature of samples from areas as small as microns (SAD) or tens of nanometers (CBED) via electron diffraction patterns. Analytical TEM can provide elemental analysis, maps and line scans using auxiliary detectors. The techniques include Energy Dispersive X-ray spectroscopy (EDS) and Electron Energy Loss Spectroscopy (EELS) which is a better technique than EDS for the identification of phases containing light elements like carbon, nitrogen, oxygen etc at high spatial resolution of ~1nm.

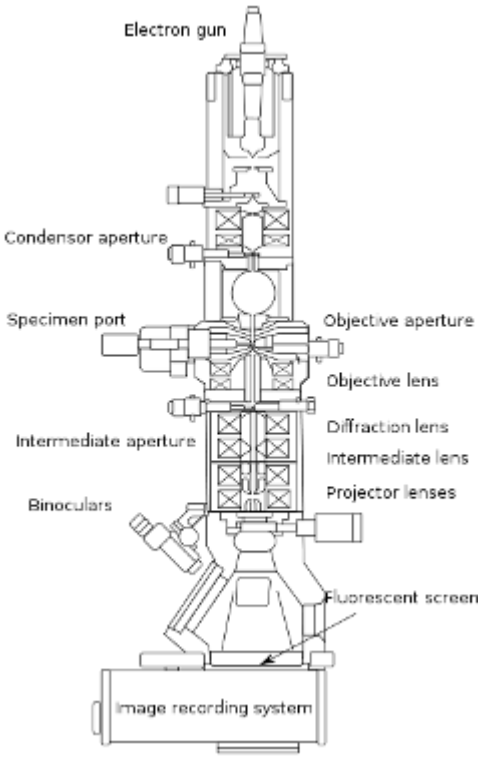

Fig. 12: Eelectron imaging system schematics of a TEM

For imaging applications, SEM can provide high quality images very quickly with significantly less sample preparation. However, TEM has substantially superior image resolution and contrast. Also, TEM does not need reference standards to provide accurate results. Therefore, TEM is widely used for process development and failure analysis of nanometer scale structures and devices, for crystallographic characterization in nanometer to micron regime and observation of defects in crystalline materials. It is also used for the characterization of nano particles in analyzing agglomeration, effects of annealing, dispersion in a matrix etc.

A schematic diagram of a typical TEM is shown in Fig. 12. From the top down, the TEM consists of an electron emission source, which may be a tungsten filament, or a lanthanum hexaboride (LaB_6) source [9]. Connecting this gun to a high voltage source (typically 100-300 kV) will give sufficient electron current either by thermionic or field emmision into the vacuum. The upper lenses of the TEM allow for the formation of the electron probe to the desired size and location for later interaction with the sample [10].

Typically a TEM consists of three stages of lensing. The stages are the condenser lenses, the objective lenses, and the projector lenses. The condenser lenses are responsible for primary beam formation, whilst the objective lenses focus the beam down onto the sample itself. The projector lenses are used to expand the beam onto the phosphor screen or other imaging device such as photographic film. The magnification of the TEM is due to the ratio of the distances between the specimen and the objective lens' image plane [11].

Bright Field and Dark Field Images: As mentioned earlier, both bright field and dark field images can be viewed in a TEM. The most common mode of operation is the bright field imaging mode. In this mode the contrast formation, when considered classically, is formed directly by occlusion and absorption of electrons in the sample. Thicker regions of the sample, or regions with a higher atomic number will appear dark, whilst regions with no sample in the beam path will appear bright – hence the term "bright field". The image is in effect assumed to be a simple two dimensional projection of the sample down the optic axis.

Samples can exhibit diffraction contrast, whereby the electron beam undergoes Bragg scattering, which in the case of a crystalline sample disperses electrons into discrete locations in the back focal plane. By the placement of apertures in the back focal plane, i.e. the objective aperture, the desired Bragg reflections can be selected (or excluded), thus only parts of the sample that are causing the electrons to scatter to the selected reflections will end up projected onto the imaging apparatus.

If the reflections that are selected do not include the un-scattered beam (which will appear up at the focal point of the lens), then the image will appear dark wherever no sample scattering to the selected peak is present, as such a region without a specimen will appear dark. This is known as a “dark-field” image.

Modern TEMs are often equipped with specimen holders that allow the user to tilt the specimen to a range of angles in order to obtain specific diffraction conditions, and apertures placed above the specimen allow the user to select electrons that would otherwise be diffracted in a particular direction from entering the specimen.

Besides observing the microstructure on a fine scale, TEM applications include the identification of lattice defects in crystals. By carefully selecting the orientation of the sample, it is possible not just to determine the position of defects but also to determine the type of defect present.

Sample Preparation Techniques for TEM

Sample preparation is an important step of any microscopic analysis and in particular, for the TEM analysis. To produce high quality TEM images, the sample needs to be thinned to 40-150 nm thick, while keeping the damage to a minimum. These techniques include:

Chemical – chemical polishing, electropolishing, full bath chemical thinning, full bath electrolytic thinning, twin jet chemical thinning, twin jet electrolytic thinning; Mechanical – Mechanical polishing, dimpling, ultrasonic grinding, wheel or wire sawing, ultra microtomy including cryo-ultramicrotomy, wedge cleavage, tripod polishing; Ion thinning including focused ion beam thinning. Specific techniques for dispersed or ultra fine materials include fine particle dispersion and frozen hydrated film of single particles.

Materials that have dimensions small enough to be electron transparent, such as powders or nano-tubes, can be quickly prepared by the deposition of a dilute sample containing the specimen onto support grids or films. In the biological sciences in order to withstand the instrument vacuum and facilitate handling, biological specimens can be fixated using either a negative staining material such as uranil acetate or by plastic embedding. Alternately samples may be held at liquid nitrogen temperatures after embedding in vitreous ice [12]. In materials science and metallurgy the specimens tend to be naturally resistant to vacuum, but still must be prepared as a thin foil, or etched so that some portion of the specimen is thin enough for the beam to penetrate. Constraints on the thickness of the material may be limited by the scattering cross section of the atoms from which the material is comprised.

Microtome (Tissue sectioning): By passing samples over a glass or diamond edge, small, thin sections can be readily obtained using a semi-automated method [13]. This method is used to obtain thin, minimally deformed samples that allow for the observation of tissue samples. Additionally inorganic samples have been studied, such as aluminium, although this usage is limited owing to the heavy damage induced in the less soft samples [14]. To prevent charge build-up at the sample surface, tissue samples need to be coated with a thin layer of conducting material, such as carbon, where the coating thickness is several nanometers. This may be achieved via an electric arc deposition process using a sputter coating device.

Sample staining: Details in light microscope samples can be enhanced by stains that absorb light. Similarly TEM samples of biological tissues can utilize high atomic number stains to enhance contrast. The stain absorbs electrons or scatters part of the electron beam which otherwise is projected onto the imaging system. Compounds of heavy metals such as osmium, lead or uranium may be used prior to TEM observation to selectively deposit electron dense atoms in or on the sample in desired cellular or protein regions. This requires an understanding of how heavy metals bind to biological tissues.

Mechanical milling: Mechanical polishing may be used to prepare samples. Polishing needs to be done to a high quality, to ensure constant sample thickness across the region of interest. A diamond, or cubic boron nitride polishing compound may be used in the final stages of polishing to remove any scratches that may cause contrast fluctuations due

to varying sample thickness. Even after careful mechanical milling, additional fine methods such as ion etching may be required to perform final stage thinning.

Chemical etching: Certain samples, particularly metallic specimens, may be prepared by chemical etching. These samples are thinned using a chemical etchant such as an acid. For controlling the thinning process, either the voltage or current passing through the specimen is varied. Systems to detect when the sample has been thinned to the required level of optical transparency are in vogue.

Ion etching: Ion etching is a sputtering process that can remove very fine quantities of material. This method is used to perform a finishing polish of specimens polished by other means. Ion etching uses an inert gas like argon passed through an electric field of a few kilovolts to generate a plasma stream that is directed to the sample surface. The sample is often rotated to promote even polishing of the surface. The sputtering rate of such methods is on the order of tens of micrometers per hour, limiting the method to only extremely fine polishing.

More recently, focused ion beam (FIB) methods have been used to prepare samples. Because FIB can be used to micro-machine samples very precisely, it is possible to mill very thin membranes from a specific area of interest in a sample, such as a semiconductor or metal. Unlike inert gas ion sputtering, FIB makes use of significantly more energetic gallium ions and may alter the composition or structure of the material through gallium implantation [12]. Fig. 13 shows the SEM image of TEM sample prepared by FIB.

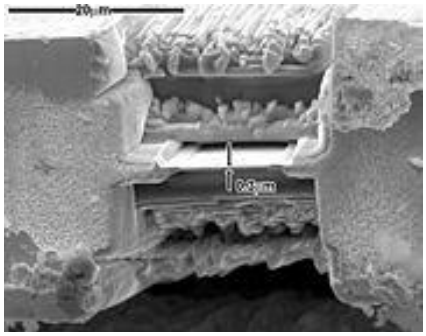

Fig.13: SEM image of a thin TEM sample milled by FIB. The thin membrane shown here is suitable for TEM examination; however, at ~300 nm thick, it would not be suitable for high-resolution TEM without further milling.

Some Typical Examples of EM Applications

The following examples are by no means exhaustive and are meant to illustrate the usefulness of the various electron microscopic and electron diffraction techniques.

Grain boundary images in iridium (SEM, FIM, TEM): Fig.14 provides an example relating to grain boundary structure in fcc iridium, which melts at 2455°C. Fig.14 (a) shows an SEM image of inter-granular, brittle fracture and a fracture surface region in iridium. Oxygen segregation to grain boundaries in iridium often renders them weakly bonded, encouraging brittle fracture [15]. The arrow in Fig.14 (a) (left) illustrates a region which could be characterized at the atomic level as illustrated in the FIM image in Fig.14 (b). The magnification difference between Fig.14 (a) and (b) is roughly 4 orders of magnitude. Fig.14 (c) shows a projected view of iridium grain boundary in a thin film viewed in the TEM. It illustrates grain boundary dislocation and ledge features composing the microstructure which characterizes the grain boundary as an interfacial region separating two different crystals or crystal orientations. Taken together the SEM, FIM, and TEM image components of Fig.14 provide an overview of the micro and nano-structure of iridium grain boundaries in a very general sense.

Nanostructures for Multiwall Carbon Nanotubes (SEM, TEM, HRTEM): Although multi wall carbon nano-tubes have only been recognized over the past 2 decades [16, 17] and their concentric graphene (carbon) tube structure observed by HRTEM [18] they have been a component of combustion regimes such as methane (CH4) or natural as combustion in the environment in antiquity [19] and have more recently been identified as environmental nano-pollutants in both the indoor [20, 21] and outdoor [22, 23] air. Fig.15(a) illustrates a variety of multi wall carbon nano-tubes in aggregated, multi concentric fullerenes collected by thermal precipitation [24] above a natural gas (~96% CH4) burner in a kitchen and observed in the TEM. An HRTEM insert Fig.15 (a) shows a 13-layer multi wall carbon nano-tube with concentric tube spacing of ~0.34 nm, which corresponds to the graphite (002) plane spacing represented in the SAED pattern insert in Fig.15 (a) The image fringe intensity contrast which decreases from the outside to the tube inside is simulated in the sketch of Fig.15(b) which also illustrates the tube chirality ($0<\theta<30°$) characterized by zig zag tubes ($\theta=0$) and armchair tubes ($\theta=30°$). Correspondingly, Fig.15(c) and (d) show chicken-wire simulations for zig zag and armchair tubes,

respectively, while Fig.15(d) also represents a chiral ($\theta \cong 15°$) tube growing over an armchair ($\theta = 30°$) tube. Lair, et al. [25,26] have recently demonstrated in computer simulations and ab initio calculations based on quantum mechanics that carbon nano tubes grow homogeneously (in carbon vapor) from a hemispherical cap (nucleus) with various configurations containing 6, 5-member (pentagonal) rings, and the growing tube end is then capped for energetic reasons. Furthermore, unlike the example shown in Fig.15 (d) the outer tube(s) grow slightly more rapidly than the inner tube(s); and the growing tubes are energetically favored to be armchair [27]. In looking at Fig.15 (a) the variance in tube diameters and tube length, as well as the end cap facets of very large diameter tubes, represents an extraordinary process of growth even in the context of gas flame combustion. The fact that carbon nano tube growth in heterogeneous nucleation processes has been achieved [28, 29] is correspondingly a remarkable phenomenon which poses unique prospects for advanced materials and materials system production and development.

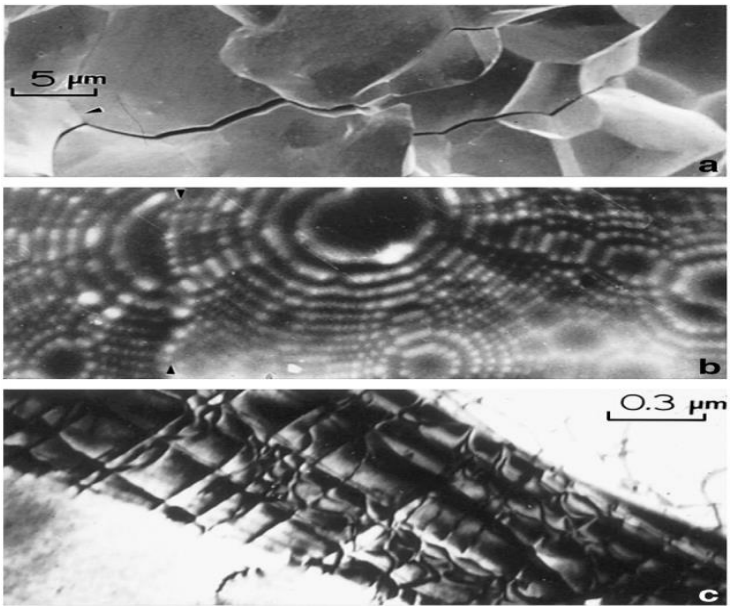

Fig. 14: Examples of grain boundary microstructures and nanostructures in fcc iridium.
(a) SEM image of inter-granular fracture features.
(b) FIM image approximating a grain boundary regime indicated at arrow (left) in (a). Liquid nitrogen (~78 K) cooling.
(c) Projected TEM image for an inclined grain boundary showing dislocation-ledge microstructure [15].

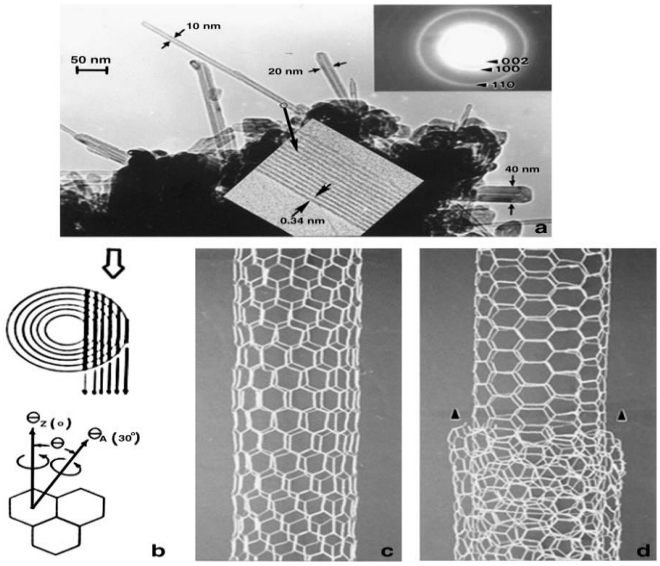

Fig. 15: Nanostructure images and image feature schematics for multi wall carbon nano-tubes (MWCNTs). (a) TEM images of MWCNTs and other multi-concentric fullerene aggregates collected from a natural gas kitchen burner by thermal precipitation [20]. Inserts show the corresponding SAED (graphite) pattern (upper etch) and a lattice-type image for the aperture over the (002) diffraction ring which corresponds to half the c-axis graphite dimension (or lattice parameter: C=0.68 nm). This image insert shows beam absorption at the inner tube decreasing outward. The explanation

for this is implicit in the upper schematic in (b). The lower schematic in (b) illustrates carbon nano-tube types: zig-zag when the axis θz(o) is the tube axis and armchair, when θA(30°) is the tube axis. Tubes with axes between 0° and 30° are referred to as chiral. (c) and (d) show chicken *w*ire models for a zig-zag tube (c) and an armchair tube over which a chiral (θ≈15°) tube is growing (arrows). The outer, concentric tubes actually grow faster than the inner tubes.

Fig.16: gives a TEM picture of polio virus which are in the nano-scale. Fig.17 shows typical dislocations on a particle.

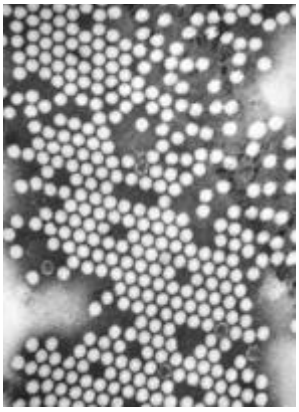

Fig.16: TEM image of the polio virus. The polio virus is 30 nm in size.

Fig.17: Transmission Electron Micrograph of dislocations which are faults in the structure of the crystal lattice at the atomic scale

Selected Area Diffraction (SAD): As previously stated, by adjusting the magnetic lenses such that the back focal plane of the lens rather than the imaging plane is placed on the imaging apparatus, a diffraction pattern can be generated. For thin crystalline samples, this produces an image that consists of a pattern of dots in the case of a single crystal, or a series of rings in the case of a polycrystalline or amorphous solid. For the single crystal case the diffraction pattern is dependent upon the orientation of the specimen and the structure of the sample illuminated by the electron beam. This image provides information about the space group symmetries in the crystal and the crystal's orientation to the beam path. Fig. 18 shows a diffraction pattern from an fcc crystal.

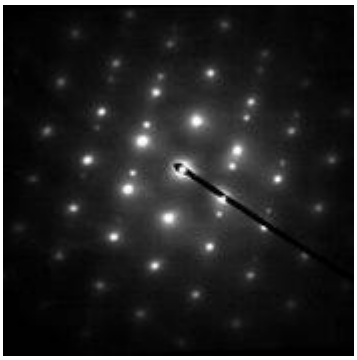

Fig.18: Crystalline diffraction pattern from a twinned grain of FCC Austenitic steel

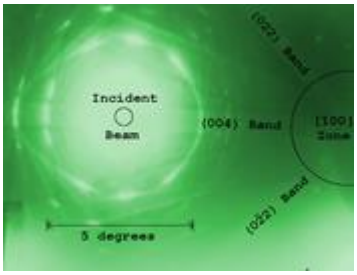

Fig.19: Convergent Beam Kikuchi lines from Silicon, near the [100] zone axis

More complex behavior in the diffraction plane is also possible, with phenomena such as Kikuchi lines arising from multiple diffraction within the crystalline lattice (Fig.19). In convergent beam electron diffraction (CBED) where a non-parallel, i.e. converging, electron wave front is produced by concentrating the electron beam into a fine probe at the sample surface, the interaction of the convergent beam can provide information beyond structural data such as sample thickness.

Examples of CBED patterns (Cu and Si(111) are given below(Fig.20)

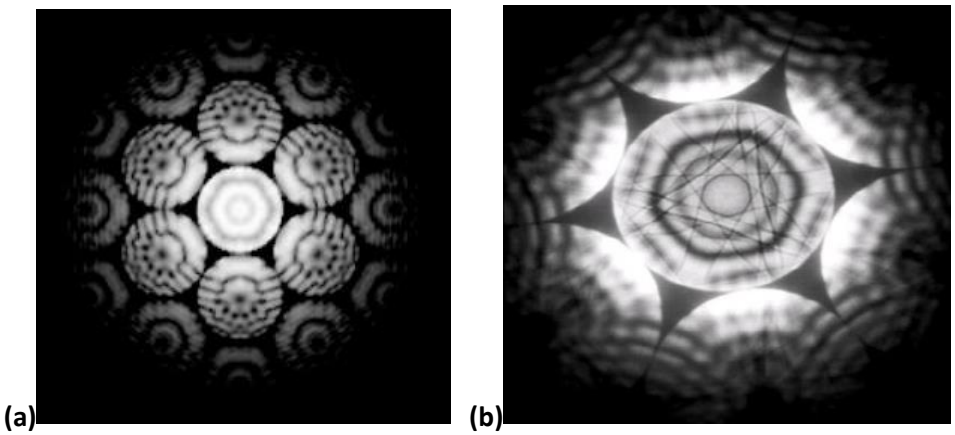

Fig.20: Examples of CBED pattern for (a) Cu and (b) Si

In the following section, some of the TEM applications from authors work are presented.

Synthesis of Cu_2O nanoparticles by chemical reduction of aqueous – colloidal dispersion of p-aminobenzoate intercalated copper hydroxysalt:

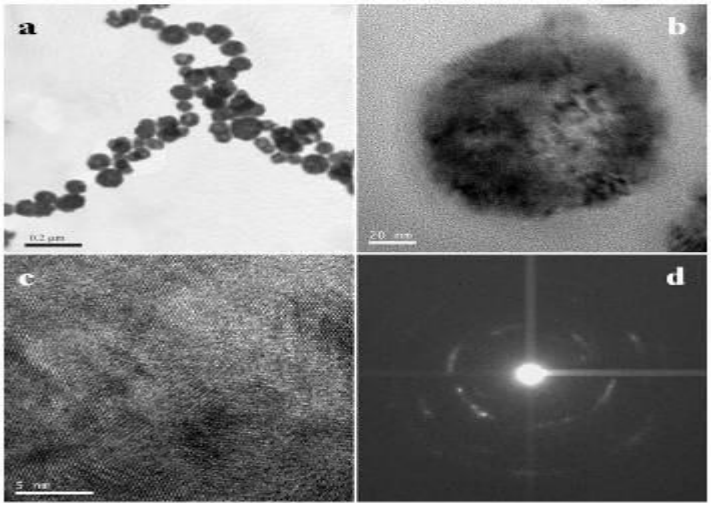

Fig.21: TEM images of Cu_2O nanoparticles obtained on reduction of the colloidal dispersion of PABA intercalated copper hydroxysalt using 0.1 M alkaline solutions of ascorbic acid - chains of Cu_2O particles (a) a single particle (b) HRTEM of a single particle (c) and SAED pattern of a single particle (d)

The bright field images of Cu_2O particles obtained on reduction of colloidal dispersion using ascorbic acid (Fig.21a) shows chains of particles ranging in diameters from 50 nm to 120 nm. An individual particle shown in Fig.21b indicates that each particle is an agglomerate of much smaller particles of diameter less than 10 nm. The high resolution image (Fig. 21c) confirms that each large particle is polycrystalline. The electron diffraction pattern (Fig. 21d) of the particle can be indexed to the cubic Cu_2O phase [JCPDS-PDF-5-0667]. The formation of polycrystalline agglomerates can be explained as follows. Reduction of individual layers of the hydroxysalt generates a number of Cu_2O nuclei in close proximity. These nuclei grow in proximity resulting in the collection of ~ 7nm particles into ~ 100nm agglomerates. [30]

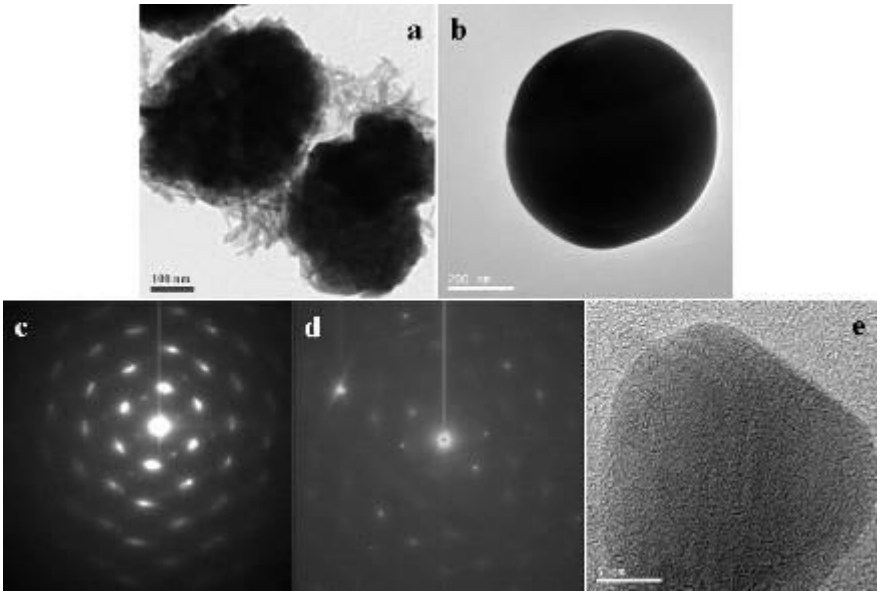

Fig.22: TEM images of Cu_2O nanoparticles obtained on reduction of the colloidal dispersion of PABA intercalated copper hydroxysalt using 0.1 M alkaline solutions of hydrazine – irregular Cu_2O particles (a) a single particle after collapse (b) SAED pattern of single particle before (c) and after (d) collapse. HRTEM of a single particle before collapse (e)

The bright field image of Cu_2O obtained by the reduction of colloidal dispersion with hydrazine shown in Fig.22a shows much larger particles (~ 300 nm). Each particle is surrounded by flake-like structures possibly due to unreacted hydroxysalt layers. The irregularly shaped particles decompose under the electron beam leading to the formation of spherical particles (Fig.22b). The electron diffraction patterns (Fig.22c and d) before and after electron beam induced decomposition are identical and these can be indexed to Cu_2O.The HRTEM image (Fig.22e) shows that these particles are also polycrystalline [30].

A few more examples are given below in support of the TEM applications for powder nano-materials from authors work (Fig.23 to 26). Fig.23 gives silver nano-particles in aqueous solution. Fig.24 gives pictures of silver nano particles prepared from different synthesis procedures [31]. Fig.25 is a typical example of nano materials for drug delivery applications and Fig.26 gives TEM pictures of CdS nano particles [32].

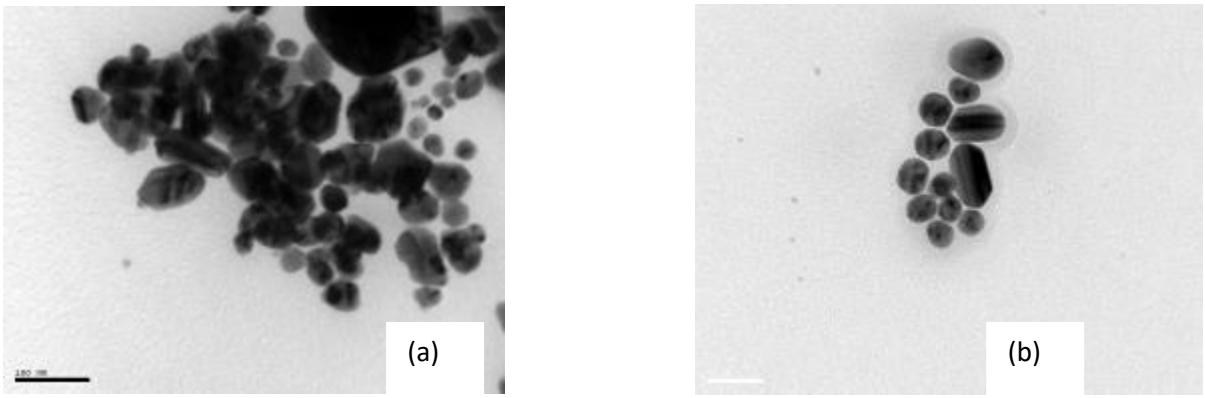

Fig.23: TEM picture of aqueous silver nano particles (a) bunch, (b) separated

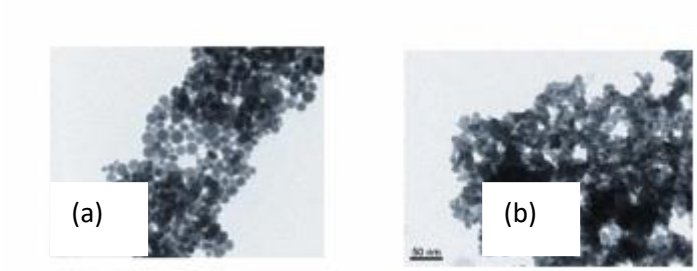

Fig.24: Transmission electron micrograph of silver nano-particles prepared in (a) 0.5 molar and (b) 1 molar solutions of TGA in DMF.

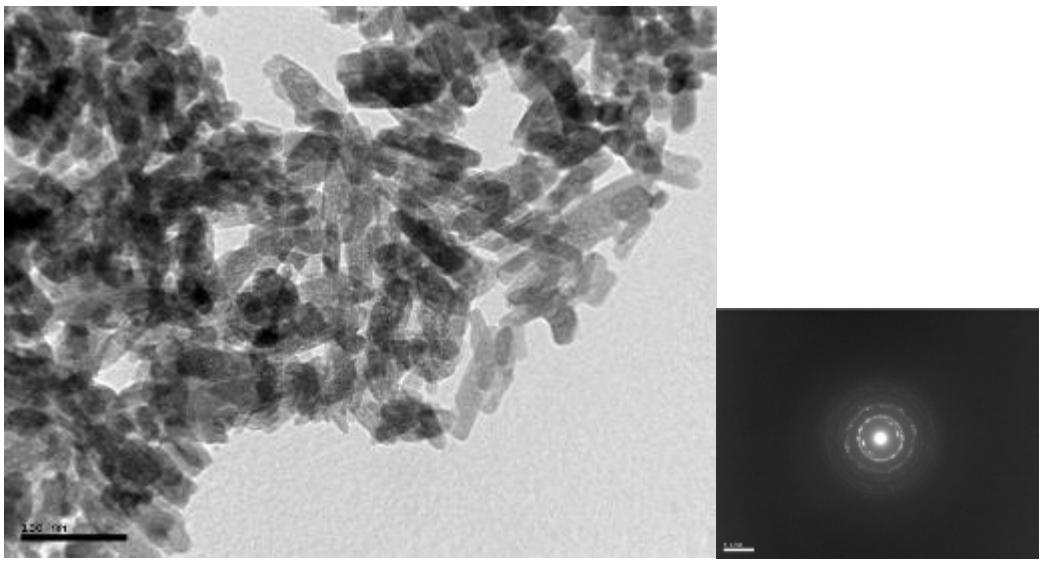

Fig.25: TEM picture of Zn doped ciprofloxacin drug with hydroxyapalite and diffraction pattern

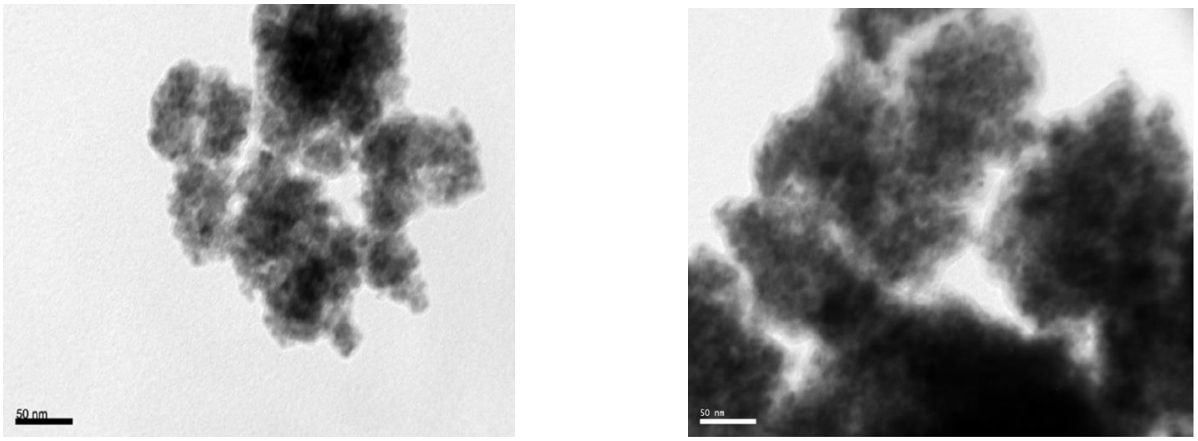

Fig.26: TEM images of precipitated CdS nanoparticles with different progress times (a) after 5 h and (b) after 1000 h.

Electron Energy Loss Spectrometry (EELS)

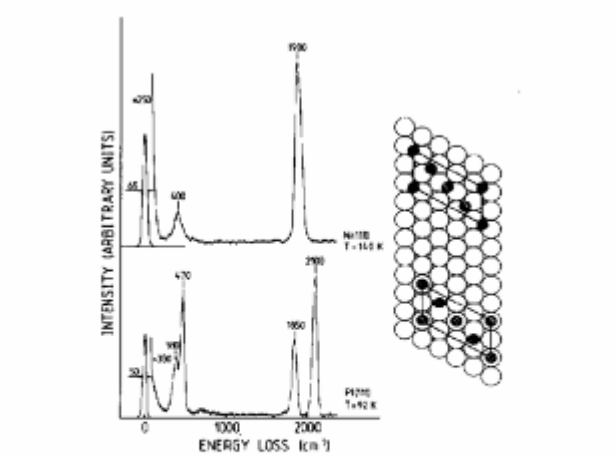

Electron energy loss spectra of the Ni(111) and Pt(111) surfaces, each covered with half a monolayer of CO which orders into a c(4 × 2) overlayer. On the nickel surface the vibration spectrum indicates only a single CO species in a site of high symmetry. The only possibility for positioning the two-dimensional CO lattice on the surface consistent with the single type of adsorption site is to place all CO molecules into twofold bridges. By similar reasoning, half the CO molecules must occupy on-top sites on the Pt(111) surface. This example shows how powerful the in situ comparison of vibrational spectra and diffraction pattern can be, since a qualitative structure analysis is achieved without analyzing diffraction intensities.

Fig.27: An example of EELS plot of Ni and Pt

An EEL is the study of the vibrational motion of atoms and molecules on and near the surface by the analysis of the energy spectrum of low-energy electrons backscattered from it. An electron passing through material can interact with electron clouds of the atoms present and transfer some of its kinetic energy to them. EELS - uses electrons from 0.1 to 10 keV and passes them through a thin foil of the material of interest. At high energies, the transmitted beam contains inelastically scattered electrons whose energy has been decreased by amounts corresponding to characteristic absorption frequencies in the solid. At lower energies, the reflected beam is monitored for the same transitions. Bulk and surface plasmons are the principal features of these spectra. An example is shown in Fig.27.

Scanning Tunneling Microscopy (STM)

A scanning tunneling microscope (STM) is a powerful instrument for imaging surfaces at the atomic level. Its development in 1981 earned its inventors, Gerd Binnig and Heinrich Rohrer (at IBM Zürich), the Nobel Prize in Physics in 1986 [33,34]. The STM is based on the concept of quantum tunneling. When a conducting tip is brought very near to the surface to be examined, a bias (voltage difference) applied between the two can allow electrons to tunnel through the vacuum between them. The resulting *tunneling current* is a function of tip position, applied voltage, and the local density of states (LDOS) of the sample [35]. Information is acquired by monitoring the current as the tip's position scans across the surface, and is usually displayed in image form. STM requires extremely clean and stable surfaces, sharp tips, excellent vibration control, and sophisticated electronics.

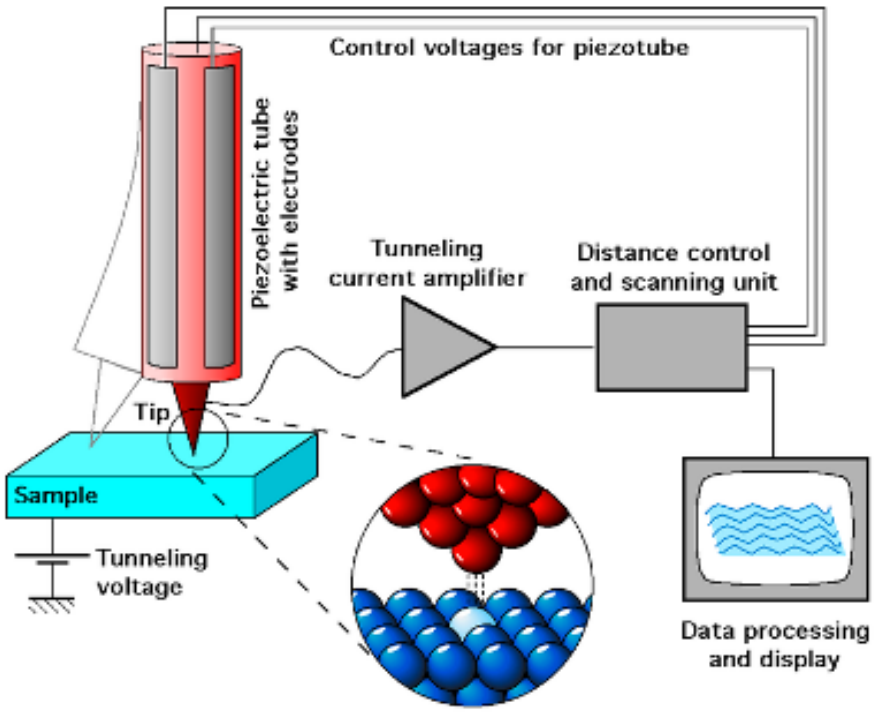

Fig.28: Schematic view of an STM

A schematic view of an STM is given in Fig. 28. The components of an STM include scanning tip, piezoelectric controlled height and x,y scanner, coarse sample-to-tip control, vibration isolation system, and computer [36]. The tip is often made of tungsten or platinum-iridium, though gold is also used. Tungsten tips are usually made by electrochemical etching, and platinum-iridium tips by mechanical shearing.

In actul operation of an STM, change in current with respect to the position of the tip can be measured itself, or the height, z, of the tip corresponding to a constant current can be measured. These two modes are called constant height mode and constant current mode, respectively. In constant current mode, feedback electronics adjust the height by a voltage to the piezoelectric height control mechanism [36]. This leads to a height variation and thus the image comes from the tip topography across the sample and gives a constant charge density surface; this means contrast on the image is due to variations in charge density [37]. In constant height mode, the voltage and height are both held constant while the current changes to keep the voltage from changing; this leads to an image made of current changes over the surface, which can be related to charge density [37]. The benefit of using a constant height mode is that it is faster, as the piezoelectric movements require more time to register the change in constant current mode than the voltage response in constant height mode [37]. All images produced by STM are grayscale, with color optionally added in post-processing in order to visually emphasize important features. The STM can be used not only in ultra high vacuum but also in air, water, and various other liquid or gas ambients, and at temperatures ranging from near zero kelvin to a few hundred degrees Celsius [35].

A good resolution for an STM is considered to be 0.1 nm lateral resolution and 0.01 nm depth resolution [38]. With this resolution, individual atoms within a sample can easily be imaged and manipulated. The resolution of an image is limited by the radius of curvature of the scanning tip. Additionally, image artifacts can occur if the tip has two tips at the end rather than a single atom; this leads to “double-tip imaging,” a situation in which both tips contribute to the tunneling. Therefore it has been essential to develop processes for consistently obtaining sharp, usable tips. Recently, carbon nanotubes have been used in this instance [39].

Due to the extreme sensitivity of tunnel current to height, proper vibration isolation or an extremely rigid STM body is imperative for obtaining usable results. In the first STM by Binnig and Rohrer, magnetic levitation was used to keep the STM free from vibrations; now mechanical spring or gas spring systems are often used.

Two STM images are shown in Figs.29, 30.

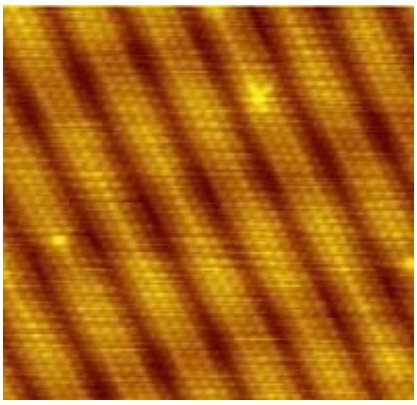

Fig.29: STM image of reconstruction on a clean gold (100) surface

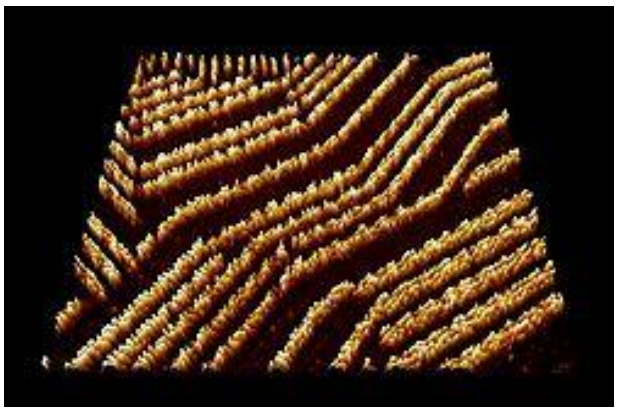

Fig.30: STM image of self-assembled supra-molecular chains of the organic semiconductor quinacridone on graphite

In addition to scanning across the sample, information on the electronic structure at a given location in the sample can be obtained by sweeping voltage and measuring current at a specific location. This type of measurement is called *scanning tunneling spectroscopy* (STS) and typically results in a plot of the local density of states as a function of energy within the sample. The advantage of STM over other measurements of the density of states lies in its ability to make extremely local measurements: for example, the density of states at an impurity site can be compared to the density of states far from impurities [40]. Framerates of at least 1 Hz enable so called Video-STM (up to 50 Hz is possible) [41,42]. This can be used to scan surface diffusion [43].

Many other microscopy techniques have been developed based upon STM. These include photon scanning microscopy (PSTM), which uses an optical tip to tunnel photons; scanning tunneling potentiometry (STP), which measures electric potential across a surface; spin polarized scanning tunneling microscopy (SPSTM), which uses a ferromagnetic tip to tunnel spin-polarized electrons into a magnetic sample [44], and atomic force microscopy (AFM), in which the force caused by interaction between the tip and sample is measured.

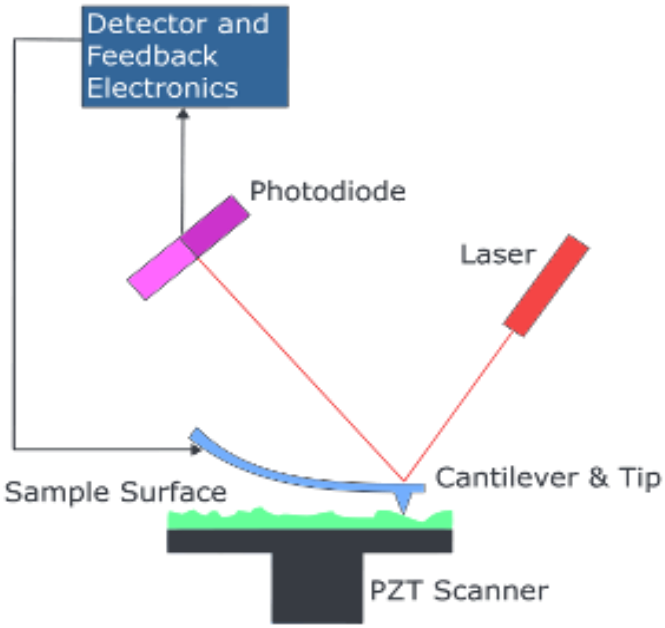

Fig.31: Block diagram of atomic force microscope

The atomic force microscope (AFM), or scanning force microscope (SFM) as it is called sometimes, is a very high-resolution type of scanning probe microscopy, with a resolution of fraction of a nanometer. The information is gathered by "feeling" the surface with a mechanical probe. Piezoelectric elements that facilitate tiny but accurate and precise movements in response to an electric command enable a very precise scanning. The atom at the apex of the tip "senses" individual atoms on the underlying surface when it forms incipient chemical bonds with each atom. Because these chemical interactions subtly alter the tip's vibration frequency, they can be detected and mapped. This principle was used to distinguish between atoms of silicon, tin and lead on an alloy surface [45]. It is one of the foremost tools for imaging, measuring, and manipulating matter at the nanoscale. One such example is given in Fig.32.

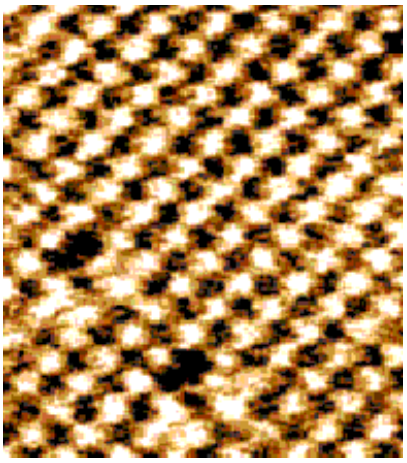

Fig.32: The atoms of a sodium chloride crystal viewed with an atomic force microscope

There are two types of operation in AFM. They are illustrated in Fig. 33 and briefly described below.

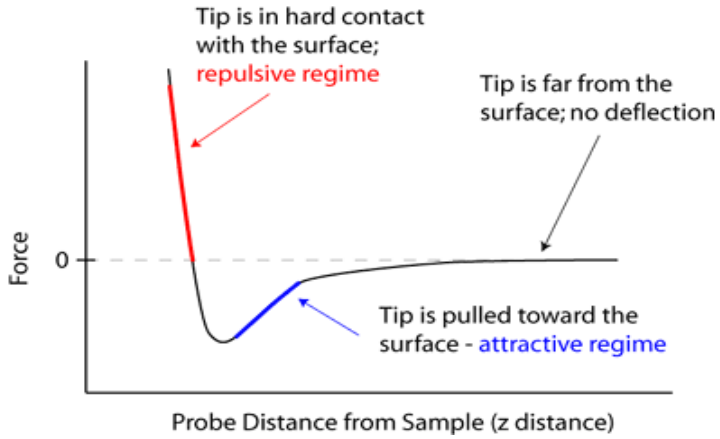

Fig.33: AFM Modes of operation

Contact Mode: The first and foremost mode of operation, contact mode is widely used. As the tip is raster-scanned across the surface, it is deflected as it moves over the surface corrugation. In constant force mode, the tip is constantly adjusted to maintain a constant deflection, and therefore constant height above the surface. It is this adjustment that is displayed as data. However, the ability to track the surface in this manner is limited by the feedback circuit. Sometimes the tip is allowed to scan without this adjustment, and one measures only the deflection. This is useful for small, high-speed atomic resolution scans, and is known as variable-deflection mode. Lateral Force Microscopy (LFM) measures frictional forces on a surface. By measuring the "twist" of the cantilever, rather than merely its deflection, one can qualitatively determine areas of higher and lower friction.

Non-contact mode: Non-contact mode belongs to a family of AC modes, which refers to the use of an oscillating cantilever. A stiff cantilever is oscillated in the attractive regime, meaning that the tip is quite close to the sample, but not touching it (hence, "non-contact"). The forces between the tip and sample are quite low, on the order of pN (10^{-12} N). The detection scheme is based on measuring changes to the resonant frequency or amplitude of the cantilever.

Focused Ion Beam (FIB) Technique

Focused ion beam is a system consisting of a SEM and a scanning gallium ion beam. This system can be used for a number of micro/nanometer scale machining tasks, from sample preparation for TEM analysis, to micromachining and repairing MEMS. It is useful in analyzing layered structures. An FIB setup is shown in Fig.34. It resembles a SEM. However, while the SEM uses a focused beam of electrons to image the sample in the chamber, an FIB setup instead uses a focused beam of ions. FIB can also be incorporated in a system with both electron and ion beam columns, allowing the same feature to be investigated using either of the beams.

Fig.34: Photograph of a FIB workstation

Most FIB instruments use liquid-metal ion sources (LMIS), especially gallium ion sources. Ion sources based on elemental gold and iridium are also available. In a gallium LMIS, gallium metal is placed in contact with a tungsten needle and heated. Gallium wets the tungsten, and a huge electric field (greater than 10^8 volts per cm) causes ionization and field emission of the gallium atoms. Source ions are then accelerated to an energy of 5-50 keV and focused onto the sample by electrostatic lenses. LMIS produce high current density ion beams with very small energy spread. A modern FIB can deliver tens of nanoampers of current to a sample, or can image the sample with a spot size on the order of a few nanometers. The principle of FIB is shown in Fig.35.

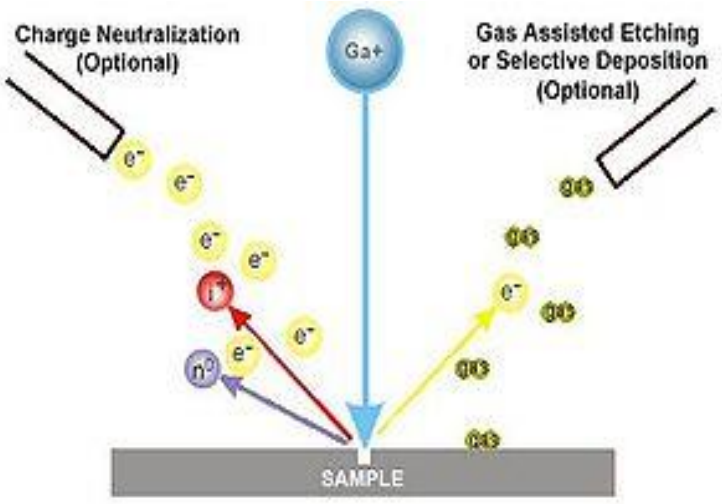

Fig.35: The principle of FIB

As the diagram shows, the gallium (Ga+) primary ion beam hits the sample surface and sputters a small amount of material, which leaves the surface as either secondary ions (i+ or i-) or neutral atoms (n^0). The primary beam also produces secondary electrons (e^-). As the primary beam rasters on the sample surface, the signal from the sputtered ions or secondary electrons is collected to form an image.

At low primary beam currents, very little material is sputtered; modern FIB systems can easily achieve 5 nm imaging resolution (world record: 2.5 nm with Cobra FIB from Orsay Physics). At higher primary currents, a great deal of material can be removed by sputtering, allowing precision milling of the specimen down to a sub micron scale.

If the sample is non-conductive, a low energy electron flood gun can be used to provide charge neutralization. In this manner, by imaging with positive secondary ions using the positive primary ion beam, even highly insulating samples may be imaged and milled without a conducting surface coating, unlike in a SEM.

Until recently, the overwhelming usage of FIB has been in the semiconductor industry. Such applications as defect analysis, circuit modification, mask repair and transmission electron microscope sample preparation of site specific locations on integrated circuits have become commonplace procedures. The latest FIB systems have high resolution imaging capability; this capability coupled with in situ sectioning has eliminated the need, in many cases, to examine FIB sectioned specimens in the SEM [46].

The most fundamental difference between FIB and focused electron beam techniques such as SEM, STEM or EBID is the use of ions instead of electrons, and this has major consequences for the interactions that occur at the sample surface. Because ions are much larger than electrons, they cannot penetrate within individual atoms of the sample. Interaction mainly involves outer shell interaction rsulting in atomic ionization and breaking of chemical bonds of the substrate atoms. Figs. 36-38 give some examples of FIB applications.

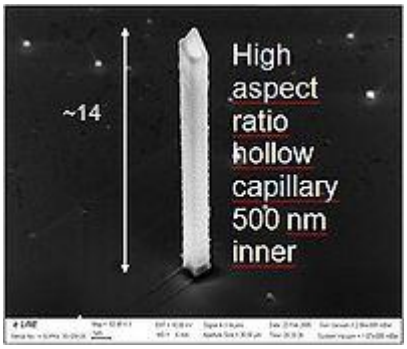

Fig.36: Example of a 3D nanostructure that can be obtained

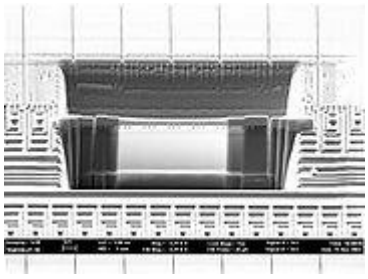

Fig.37: SEM image of a thin TEM sample milled by FIB

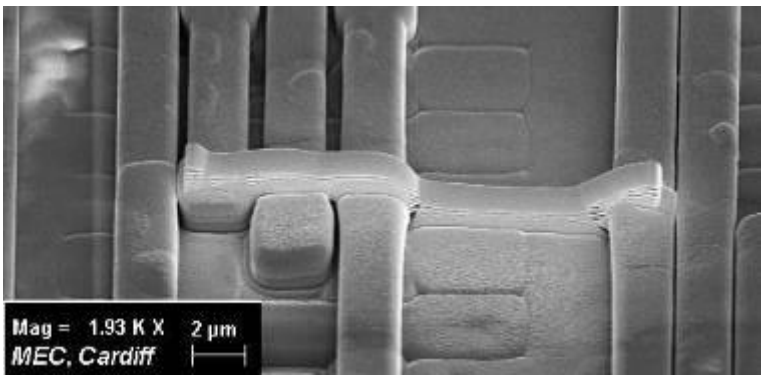

Fig.38: FIB chip repair. The image shows an added Pt stripe through FIB gas assisted deposition, which serves as electrical connector

FIB is often used in the semiconductor industry to patch or modify an existing semiconductor device. For example, in an integrated circuit, the gallium beam could be used to cut unwanted electrical connections, and/or to deposit conductive material in order to make a connection. The high level of surface interaction is exploited in patterned doping of semiconductors. FIB is also used for mask-less implantation. An important application lies in its use to prepare samples for the transmission electron microscope. TEM requires very thin samples, typically ~100 nanometers. Other techniques, such as ion milling or electro-polishing can be used to prepare such thin samples. However, the nanometer-scale resolution of the FIB allows the exact thin region to be chosen. This is vital, for example, in integrated circuit failure analysis. FIB preparation can be used with cryogenically frozen samples in a suitably equipped instrument, allowing cross sectional analysis of samples containing liquids or fats, such as biological samples, pharmaceuticals, foams, inks, and food products [47].

The drawbacks to FIB sample preparation are the surface damage and implantation, which produce noticeable effects when using techniques such as high-resolution "lattice imaging" TEM or electron energy loss spectroscopy. This damaged layer can be minimized by FIB milling with lower voltages or by further milling with a low-voltage argon ion beam after completion of the FIB process [48].

SUMMARY

In this paper, characterization techniques with special reference to electron microscopic techniques for nano material characterization have been elucidated with typical examples and applications. Also, sample preparation techniques for observation of materials in SEM and TEM have been discussed. The electron microscope equipment and related facilities available at Indian Institute of Science have been mentioned. Besides bringing out the applications of these techniques with supporting pictures from the literature, the author's own studies with some typical examples of pictures taken using the SEM and TEM are presented. It is hoped that the examples presented in this paper represent useful application of modern imaging techniques in solving materials science and engineering problems in nanotechnology.

REFERENCES

1. Asthana, R., Kumar, A., & Dahotre, N. B. (2006). Materials processing and manufacturing science. Elsevier.
2. Avadhani, G. S. Characterization of Nano Materials using Electron Microscopy: Invited talk in the "Indo-Russian workshop on nanotechnology and laser induced plasma (IR-NANO-2009)" November 24-26, 2009. New Delhi, India.
3. Mehta, S. K., Kumar, S., Chaudhary, S., & Bhasin, K. K. (2009). Effect of cationic surfactant head groups on synthesis, growth and agglomeration behavior of ZnS nanoparticles. Nanoscale research letters, 4(10), 1197-1208.
4. Corbari, L., Cambon-Bonavita, M. A., Long, G. J., Grandjean, F., Zbinden, M., Gaill, F., & Compère, P. (2008). Iron oxide deposits associated with the ectosymbiotic bacteria in the hydrothermal vent shrimp Rimicaris exoculata. Biogeosciences, 5(5), 1295-1310.
5. Von Ardenne M. von Ardenne M. Improvements in electron microscopes. GB patent 511204, convention date (Germany) 18 Feb (1937)
6. Suzuki, E. (2002). High-resolution scanning electron microscopy of immunogold-labelled cells by the use of thin plasma coating of osmium. Journal of microscopy, 208(3), 153-157.
7. Seligman, A. M., Wasserkrug, H. L., & Hanker, J. S. (1966). A new staining method (OTO) for enhancing contrast of lipid-containing membranes and droplets in osmium tetroxide-fixed tissue with osmiophilic thiocarbohydrazide (TCH). The Journal of cell biology, 30(2), 424.
8. Goldstein, J. I., Newbury, D. E., Echlin, P., Joy, D. C., Fiori, C., & Lifshin, E. (1981). Preparation of biological samples for scanning electron microscopy. In Scanning electron microscopy and X-ray microanalysis (pp. 495-539). Springer, Boston, MA.
9. Egerton, R Physical principles of electron microscopy. Springer. ISBN 0387258000. (2005).
10. Rose, H. H. (2008). Optics of high-performance electron microscopes. Science and Technology of Advanced Materials, 9(1), 014107.
11. The Objective lens of a TEM, the heart of the electron microscope:link:http:rodenburg.org/guide/t700.html
12. Amzallag, A., Vaillant, C., Jacob, M., Unser, M., Bednar, J., Kahn, J. D., ... & Maddocks, J. H. (2006). 3D reconstruction and comparison of shapes of DNA minicircles observed by cryo-electron microscopy. Nucleic acids research, 34(18), e125-e125.
13. Porter, K. R., & Blum, J. (1953). A study in microtomy for electron microscopy. The anatomical record, 117(4), 685-709.
14. Phillips, R. (1961). Diamond knife ultra microtomy of metals and the structure of microtomed sections. British Journal of Applied Physics, 12(10), 554.
15. Murr, L. E. (2009). Imaging systems and materials characterization. Materials characterization, 60(5), 397-414.
16. Tibbetts, G. G. (1989). Vapor-grown carbon fibers: status and prospects. Carbon, 27(5), 745-747.
17. Gao, Y. D., & Herndon, W. C. (1992). Tubular graphic carbon structures. Molecular Physics, 77(3), 585-599.
18. Iijima, S. (1991). Helical microtubules of graphitic carbon Nature 354: 56–58. Find this article online.
19. Murr, L. E., Esquivel, E. V., Bang, J. J., De La Rosa, G., & Gardea-Torresdey, J. L. (2004). Chemistry and nanoparticulate compositions of a 10,000 year-old ice core melt water. Water research, 38(19), 4282-4296.
20. Murr, L. E., Bang, J. J., Esquivel, E. V., Guerrero, P. A., & Lopez, D. A. (2004). Carbon nanotubes, nanocrystal forms, and complex nanoparticle aggregates in common fuel-gas combustion sources and the ambient air. Journal of Nanoparticle Research, 6(2), 241-251.
21. Murr, L. E., & Soto, K. F. (2005). A TEM study of soot, carbon nanotubes, and related fullerene nanopolyhedra in common fuel-gas combustion sources. Materials Characterization, 55(1), 50-65.
22. Murr, L. E., Garza, K. M., Soto, K. F., Carrasco, A., Powell, T. G., Ramirez, D. A., ... & Venzor, J. 3. (2005). Cytotoxicity assessment of some carbon nanotubes and related carbon nanoparticle aggregates and the implications for anthropogenic carbon nanotube aggregates in the environment. International journal of environmental research and public health, 2(1), 31-42.
23. Murr, L. E., Soto, K. F., Garza, K. M., Guerrero, P. A., Martinez, F., Esquivel, E. V., ... & Venzor III, J. (2006). Combustion-generated nanoparticulates in the El Paso, TX, USA/Juarez, Mexico Metroplex: their comparative

characterization and potential for adverse health effects. International journal of environmental research and public health, 3(1), 48-66.
24. Bang, J. J., Trillo, E. A., & Murr, L. E. (2003). Utilization of selected area electron diffraction patterns for characterization of air submicron particulate matter collected by a thermophoretic precipitator. Journal of the Air & Waste Management Association, 53(2), 227-236.
25. Lair, S. L., Herndon, W. C., Murr, L. E., & Quinones, S. A. (2006). End cap nucleation of carbon nanotubes. Carbon, 44(3), 447-455.
26. Lair, S. L., Herndon, W. C., & Murr, L. E. (2007). Energetic trends of single-walled carbon nanotube ab initio calculations. Journal of materials science, 42(5), 1819-1827.
27. Lair, S. L. (2007). Energetic comparison of double-walled carbon nanotube systems. The University of Texas at El Paso.
28. Ebbesen, T. W. (1996). Carbon nanotubes: preparation and properties. CRC press.
29. Schwarz, J. A., Contescu, C. I., & Putyera, K. (Eds.). (2004). Dekker encyclopedia of nanoscience and nanotechnology (Vol. 5). CRC press.
30. M.R.Rajamathi and G.S.Avadhani Synthesis of Cu2O nanoparticles by chemical reduction of aqueous – colloidal dispersion of p-aminobenzoate intercalated copper hydroxysalt: (private communication)
31. M.K. Rabinal K, Praveenkumar, M.N. Kalasad, V.R. Bharadi, A. M. Bhikshavartimath, B.G. Mulimani and G.S. Avadhani Electrochemical Synthesis and Physical Properties of Capped Silver Nanoparticles (communicated to Materials Characterization).
32. Kalasad, M. N., Rabinal, M. K., Mulimani, B. G., & Avadhani, G. S. (2008). Temporal evolution of capped cadmium sulfide nanoparticles. Semiconductor science and technology, 23(4), 045009.
33. Binnig, G., & Rohrer, H. (2000). Scanning tunneling microscopy. IBM Journal of research and development, 44(1/2), 279.
34. Prize, N. Press release for the 1986 Nobel Prize in physics, 1986.
35. Chen, J. (2021). Introduction to Scanning Tunneling Microscopy Third Edition (Vol. 69). Oxford University Press, USA.
36. Oura, K., Lifshits, V. G., Saranin, A. A., Zotov, A. V., & Katayama, M. (2013). Surface science: an introduction. Springer Science & Business Media.
37. Bonnell, D. A., & Huey, B. D. (2001). Basic principles of scanning probe microscopy. Scanning probe microscopy and spectroscopy: Theory, techniques, and applications, 7.
38. Bai, C. (2000). Scanning tunneling microscopy and its application (Vol. 32). Springer Science & Business Media.
39. Pasquini, A., Picotto, G. B., & Pisani, M. (2005). STM carbon nanotube tips fabrication for critical dimension measurements. Sensors and Actuators A: Physical, 123, 655-659.
40. Pan, S. H., Hudson, E. W., Lang, K. M., Eisaki, H., Uchida, S., & Davis, J. C. (2000). Imaging the effects of individual zinc impurity atoms on superconductivity in Bi2Sr2CaCu2O8+ δ. Nature, 403(6771), 746-750.
41. Schitter, G., & Rost, M. J. (2008). Scanning probe microscopy at video-rate. Materials Today, 11, 40-48.
42. Lapshin, R. V., & Obyedkov, O. V. (1993). Fast-acting piezoactuator and digital feedback loop for scanning tunneling microscopes. Review of scientific instruments, 64(10), 2883-2887.
43. Swartzentruber, B. S. (1996). Direct measurement of surface diffusion using atom-tracking scanning tunneling microscopy. Physical review letters, 76(3), 459.
44. Wiesendanger, R., Shvets, I. V., Bürgler, D., Tarrach, G., Güntherodt, H. J., & Coey, J. M. D. (1992). Recent advances in spin-polarized scanning tunneling microscopy. Ultramicroscopy, 42, 338-344.
45. Sugimoto, Y., Pou, P., Abe, M., Jelinek, P., Pérez, R., Morita, S., & Custance, O. (2007). Chemical identification of individual surface atoms by atomic force microscopy. Nature, 446(7131), 64-67.
46. Introduction :FocusedIonBeamSystems"http://www.fibics.com/fib/tutorials/introduction-focused-ion-beam-systems/4/. Retrieved -08-06. (2009).
47. Link:http:quorumtech.com/Applications/Cryo Apps Library/cryo-SDB.pdf Retrieved -06-06. (2009).
48. Principe, E. L., Gnauck, P., & Hoffrogge, P. (2005). A three beam approach to TEM preparation using in-situ low voltage argon ion final milling in a FIB-SEM instrument. Microscopy and Microanalysis, 11(S02), 830-831.